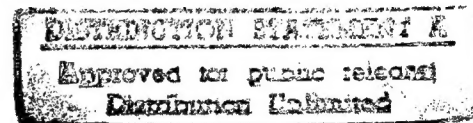




JPRS Report



Science & Technology

USSR: Materials Science

19980113 379

DTIC QUALITY INSPECTED 8

Science & Technology

USSR: Materials Science

JPRS-UMS-91-008

CONTENTS

31 October 1991

ANALYSIS, TESTING

On Technique for Estimating Residual Stresses in Railroad Rails [A. Yu. Abdurashitov, M. N. Georgiyev, et al.; <i>ZAVODSKAYA LABORATORIYA</i> , Apr 91]	1
Development of Residual Plastic Creep Deformation as Function of Stress and Temperature in Long-Term Failure of Metal Materials [V. I. Kovpak; <i>PROBLEMY PROCHNOSTI</i> , No 5, 91]	1
Critical Brittleness Temperature of High-Strength Steel for Fasteners for Use in Power Equipment Under Pressure [V. I. Gorynin; <i>PROBLEMY PROCHNOSTI</i> , No 5, 91]	1
Experimental Study of Bending of Cylindrical Shells Under Creep Conditions With Small Vibrations [S. A. Shesterikov, A. M. Lokoshchenko, et al.; <i>PROBLEMY PROCHNOSTI</i> , No 5, 91]	1

COMPOSITE MATERIALS

Mechanics of Composite Materials With Contoured Structures (A Survey). Continual Theory, Fiber Composites [S. D. Akbarov, A. N. Guz; <i>PRIKLADNAYA MEKHANIKA</i> No 5, 91]	3
---	---

CORROSION

Electrodeposition of Iron and Fe-Ni Alloys From Electrolytes Containing Ascorbic Acid [S. I. Berezina, L. G. Sharapova, et al.; <i>ZASHCHITA METALLOV</i> , Jan 91]	4
Model of Oriented Crystal Growth During Electrodeposition of Metals [N. V. Podbornov, A. I. Zhikharev, et al.; <i>ZASHCHITA METALLOV</i> , Jan 91]	4
Passivation of Chromium Steels During Isothermal Oxidation Under Low Oxygen Pressure [Ye. K. Oshe, T. Yu. Zimina, et al.; <i>ZASHCHITA METALLOV</i> , Jan 91 pp 49-54]	4
Influence of Hydroxyl and Chromate Ions on Corrosion of Carbon Steel [V. P. Isupov, I. G. Gorichev, et al.; <i>ZASHCHITA METALLOV</i> , Jan 91]	5
Cathodic Behavior of TiC and of Carbide Surface Layers on Titanium [T. V. Chukalovskaya, N. P. Chebotareva, et al.; <i>ZASHCHITA METALLOV</i> , Jan 91]	5
Formation of Titanium Coatings on Steel by Thermodiffusion From Melt [A. G. Sokolov, T. I. Ivanova, et al.; <i>ZASHCHITA METALLOV</i> , Feb 91]	6
Experience With Coating of Zinc Alloyed With Titanium [L. I. Kadaner, T. S. Bazilevich; <i>ZASHCHITA METALLOV</i> , Feb 91]	6
Behavior of Ti-Nb-Ni Alloys in Sulfuric and Hydrochloric Acids [A. I. Shcherbakov, V. N. Dorofeyeva, et al.; <i>ZASHCHITA METALLOV</i> , Feb 91]	6
Emission Characteristics and Composition of Surface Layers of Fe-Si Alloys [N. V. Kolganova, N. G. Shirina, et al.; <i>ZASHCHITA METALLOV</i> , Feb 91]	7
Tungsten Buildup on Surface of Ti-W Alloys [A. I. Shcherbakov; <i>ZASHCHITA METALLOV</i> , Feb 91]	7
Function Describing Change of Rate of Air Corrosion of Metals in Time. Effect of Atmospheric Conditions and of Alloying Elements on Corrosion Resistance of Steels and Cast Irons [Vu Din Vuy; <i>ZASHCHITA METALLOV</i> , Feb 91]	8
Effect of Polarization on Development of Ocean Bacteria During Galvanic Corrosion of Metals [Y. M. Korovin, A. V. Ledenev; <i>ZASHCHITA METALLOV</i> , Feb 91]	8
Electrochemical Behavior and Corrosion of Stainless Steels in Model Solutions of Nutrient Salts Simulating Production of Food Protein From Natural Gas [Yu. S. Ruskol, L. I. Viter; <i>ZASHCHITA METALLOV</i> , Jan 91]	9
Corrosion Resistance of 02Cr8Ni22Si6 (EP794) Low-Carbon Alloy Steel [N. A. Adugina, L. A. Andreyeva, et al.; <i>TYAZHELOYE MASHINOSTROYENIYE</i> , May 91]	9
Corrosion-Resistant Chromium Steel Without Nickel and Its Industrial Status [V. P. Borisov, M. F. Vorokhanova, et al.; <i>TYAZHELOYE MASHINOSTROYENIYE</i> , May 91]	10
Corrosion Resistance of High-Strength Cast Iron at High Temperatures in Oil Bed Water [Yu. A. Ishchuk, L. A. Solntsev, et al.; <i>ZASHCHITA METALLOV</i> , Feb 91]	10
Dependence of Electrochemical Behavior and Corrosion Characteristics of (Fe,Cr) ₈₅ B ₁₅ Alloys on Cr Content [G. V. Borisova, V. V. Maslov, et al.; <i>ZASHCHITA METALLOV</i> , Feb 91]	11

Corrosion Characteristics of Grade-45 Carbon Steel Chromized and Chromosilicized by Diffusion Process in Protective Media [O.V. Kasparova, A.A. Zorin, et al.; <i>ZASHCHITA METALLOV</i> , Feb 91]	11
Capabilities of High-Energy Surface Treatment Methods for Corrosion Protection of Metals [V.I. Kolotyrkin, V.M. Knyazheva; <i>ZASHCHITA METALLOV</i> , Feb 91]	11
Increasing Rail Protection From Electrocorrosion [A.V. Naumov; <i>ELEKTRICHESKAYA I TEPLOVOZNAYA TYAGA</i> , May 91]	12
Surface Titanium Alloying (Modification) by Laser Irradiation [N.D. Tomashov, I.B. Skvortsova, et al.; <i>ZASHCHITA METALLOV</i> , No 3, May-Jun 91]	12
On Conjoint Effect of Silicon and Carbon on Intercrystalline Corrosion in Tempered Austenite Stainless Steels in Highly Oxidizing Media [O.V. Kasparova, V.M. Milman, et al.; <i>ZASHCHITA METALLOV</i> , No 3, May-Jun 91]	13

FERROUS METALS

Rolling Steel Strip With Continuous Heating [B.Ye. Paton, B.I. Medovar, et al.; <i>PROBLEMY SPETSIALNOY ELEKTROMETALLURGII</i> , Jan-Mar 91]	14
Production Line USh-172 for Large-Scale Electroslag Chill Casting of Slabs From Liquid Charge [Yu.V. Orlovskiy, V.Ya. Maydannik, et al.; <i>PROBLEMY SPETSIALNOY ELEKTROMETALLURGII</i> , Jan-Mar 91]	14
Phase Formation in Vacuum Condensates of Binary Oxides With Titanium Oxide [V.D. Kushkov, A.M. Zaslavskiy, et al.; <i>PROBLEMY SPETSIALNOY ELEKTROMETALLURGII</i> , Jan-Mar 91]	14
Feasibility of Using Ceramic Filters for Refining Stainless Steel With Titanium Content [M.V. Rymarchuk, B.I. Shukstulskiy, et al.; <i>PROBLEMY SPETSIALNOY ELEKTROMETALLURGII</i> , Jan-Mar 91]	14

NONMETALLIC MATERIALS

Heat-Insulating Zirconium Dioxide-Based Ceramic Coating Advertised [MASHINOSTROITEL, No 3, 91]	16
Allowing for Defects When Calculating Failure Probability for Ceramic Parts Subjected to Short-Term Loading [M. I. Gorbatshevich, A. Ye. Ginsburg; <i>PROBLEMY PROCHNOSTI</i> No 4, 91]	16
Estimating the Factor of Safety for Ceramic Parts [Yu. I. Dobrinskiy; <i>PROBLEMY PROCHNOSTI</i> No 4, 91]	16

PREPARATIONS

Amorphous Materials: Powder-Forming Methods [O. V. Roman; <i>DOKLADY AKADEMII NAUK BSSR</i> No 1, 91]	17
--	----

WELDING, BRAZING, SOLDERING

Effect of High-Output Rail Cutting Methods on Resistance Welding Quality [N.A. Sinadskiy, V.B. Shlyapin; <i>SVAROCHNOYE PROIZVODSTVO</i> , May 91]	18
---	----

MISCELLANEOUS

Magnetically Controlled RAP 160/320K-10 X-Ray Unit [Ye.A. Gusev, V.P. Drankov, et al.; <i>DEFEKTOSKOPIYA</i> , Mar 91]	19
Unit for Measuring Dynamic and Quasistatic Magnetic Characteristics [M.A. Melguy, A.A. Osipov; <i>DEFEKTOSKOPIYA</i> , Mar 91]	19

On Technique for Estimating Residual Stresses in Railroad Rails

*917D0188A Moscow ZAVODSKAYA LABORATORIYA
in Russian Vol 57 No 4, Apr 91 pp 57-58*

[Article by A. Yu. Abdurashitov, M. N. Georgiyev, N. Ya. Mezhova, V. A. Reykhart, All-Union Science Research Institute of Railway Transport]

UDC 620.178.3

[Abstract] The issue of increasing the operational reliability of rails containing 0.71-0.82% C, 0.75-1.05% Mn by bulk oil quenching with subsequent tempering at 450°C for two hours is addressed and the role of resistance to the formation and propagation of fatigue cross cracks which depend on the magnitude and sign of residual stress in the crack zone is emphasized. Ways of determining residual stresses in the presence of cross cracks are examined. The technique is based on the dependence of the fracture mechanics between critical values of the notch sensitivity index, load, and crack area. The load vs. deflection curve was plotted during the tests while critical values of the notch sensitivity index were determined according to state standard GOST 25.506-85. The dependence of breaking force and nominal breaking stress on the external fatigue cross crack area is established. An evaluation of the results shows that the proposed technique makes it possible analytically to determine the level of residual stresses developing in the rail web by using critical values of the notch sensitivity index obtained by testing standard specimens and full-section rail samples. References 6; figures 1; tables 1.

Development of Residual Plastic Creep Deformation as Function of Stress and Temperature in Long-Term Failure of Metal Materials

*917D0171C Kiev PROBLEMY PROCHNOSTI
in Russian No 5, 1991 pp 91-95*

[Article by V. I. Kovpak, Institute of Strength Problems, Ukrainian Academy of Sciences]

UDC 699.15:539.376

[Abstract] The relative elongation of specimens after rupture in long-term laboratory studies is used to refine the conditions of temperature-time similarity between the characteristics of long-term strength and creep in a continuing study of the conditions required to use tests lasting not over one year to determine the long-term strength of metal materials for service lives of up to 500,000 hours. Although there is significant scattering of the characteristics of relative elongation in the failure of viscous metal materials, the variation in numerical values of the characteristic as a function of stress and temperature reveal the fundamental rules of creep resistance and long-term failure of metals, facilitating proper

selection of methods for long-term prediction of long-term strength. The assumption of Larsen and Miller among others that equivalent conditions of failure at different temperatures correspond to the same values of parameters as a function of stress $P(>s) = \text{const}$ is not confirmed by this study. In fact, the different characteristics of residual plastic deformation indicate that extrapolation of the results of shorter-term tests must also be performed by different methods. Figures 5; references 13.

Critical Brittleness Temperature of High-Strength Steel for Fasteners for Use in Power Equipment Under Pressure

*917D0171A Kiev PROBLEMY PROCHNOSTI
in Russian No 5, 1991 pp 35-37*

[Article by V. I. Gorynin, Leningrad, Central Boiler-Turbine Institute Scientific-Production Association]

UDC 669.14:620.178.74-238

[Abstract] A study is made of the influence of defects in fasteners and an impact specimen on the accuracy of determining permissible values of critical brittleness temperature of high-strength steel. Impact testing was performed at -196 - +250 °C on both prismatic and cylindrical specimens with four types of notches. An estimate is suggested for the permissible critical brittleness temperature in fasteners, based on the condition of the steel and number of defects in fasteners and the required operating life of the threaded joints. The method allows better founded requirements to be generated for serviceability of materials in the design, manufacture and use stages. Figures 3; references 3.

Experimental Study of Bending of Cylindrical Shells Under Creep Conditions With Small Vibrations

*917D0171B Kiev PROBLEMY PROCHNOSTI
in Russian No 5, 1991 pp 87-90*

[Article by S. A. Shesterikov, A. M. Lokoshchenko, Ye. A. Myakotin and N. Ye. Pechenina, Institute of Mechanics, Moscow State University]

UDC 621.17.013:620.169

[Abstract] Results are presented from an experimental study of the creep of shells in flexure as a function of additional flexural and torsional low-amplitude vibrations simultaneously applied. The test specimens were shells of D16T aluminum alloy cut from pipes. Nominal shell sizes were 36 mm diameter, 1 mm wall thickness, 350 mm gage section length. The specimens were first heated to 200 °C and held for two hours, then loaded in noncentral extension producing flexure. The shell was held for an assigned period under static conditions, then a vibrator was periodically switched on, always vibrating at 20 Hz. The periodic component of the variable stress was never over 2-3% of the

maximum static stress. The ratio of mean creep rates with and without vibration was used to provide a quantitative estimate of the integral influence of vibration on creep rate.

The presence of the small vibrations was found consistently to accelerate the creep of the shells by an average factor of 2. Figures 4; references 11.

**Mechanics of Composite Materials With
Contoured Structures (A Survey). Continual
Theory, Fiber Composites**

917D0174A Kiev PRIKLADNAYA MEKHANIKA
in Russian No 5, 1991 pp 3-20

[Abstract of article by S. D. Akbarov, A. N. Guz]

UDC 539.4

[Abstract] Previous studies of small-scale curvatures in the reinforcing elements of composite materials were surveyed. Two approaches in these studies were identified. One approach stresses the stress-strain state of areas larger than the curvatures, and the other, more recent one, the stress-strain state of areas at least one order of magnitude smaller than the curvatures. The history of continual theories was summarized in Part 1 of the article, with the main emphasis placed on the second approach. This summary was followed by a discussion in Part 2 of the development of continual theories as they apply to the mechanics of composite materials with

contoured structures. The basic premises of these theories are that 1) composite materials have regular curvatures (along the ox_1 axis at intervals of 2Λ , with Λ denoting the curvature halflength), and that 2) the nature of the curvatures satisfies the inequalities: h is much less than H ; Λ is much less than d ; and H is much less than Λ , where h is the typical minimum filler size, H is the curvature rise, and d is the minimum size of region D occupied by the body in question. Part 3 was devoted to the elaboration of a model of a piecewise-homogenous body for fiber composites. The problem was stated in terms of an infinite elastic body reinforced by any number of non-intersecting curved fibers. Determination of the stress-strain state was reduced to solving the appropriate closed equation systems. Solutions were presented for both high and low fiber concentrations, and concrete problems were examined. The authors suggested that further research into the mechanics of composites with curved structures should investigate static and dynamic problems within the framework of continual theory and how the stress-strain state in fiber composites with curved structures is affected by fiber interaction. Figures 8; references 49: 47 Russian, 2 Western.

Electrodeposition of Iron and Fe-Ni Alloys From Electrolytes Containing Ascorbic Acid

917D0140E Moscow ZASHCHITA METALLOV
in Russian Vol 27 No 1, Jan 91 pp 149-152

[Article by S.I. Berezina, L.G. Sharapova, V.P. Veselkov, and N.A. Plechnaya, USSR Academy of Sciences, Kazan branch, and Institute of Organic and Physical Chemistry imeni A.Ye. Arbuzov]

UDC 621.357.7

[Abstract] Electrodeposition of iron and Fe-Ni alloys from electrolytes containing ascorbic acid and Fe(II) salt in equimolar amounts is evaluated, the role of ascorbic acid being to prevent formation of iron hydroxides in the cathodic surface layer. Experiments were performed with 0.5 mol.% FeSO_4 + 0.5 mol.% H_2Asc solutions (pH 2.1-5.9) and also with 0.5 mol.% FeSO_4 + 0.5 mol.% H_2Asc + 0.5 mol.% H_3Cit solutions (pH 4.0-8.2) at room temperature. The current efficiency of Fe yield from the FeSO_4 -Asc solutions was found to reach and exceed 95 % at 1.0-1.5 A/dm² current densities, then to drop to 44 % and much lower upon addition of citric acid. Nickel was then electrodeposited from 0.9 mol.% NiCl_2 + 0.9 mol.% H_2Asc solutions (pH 4-6), with 70-95 % current efficiencies of Ni yield at 0.25-8.0 A/dm² current densities. In the last experiment nickel and iron were codeposited from two equimolar Fe(II) and Ni(II) solutions containing ascorbic acid: 0.5 mol.% FeSO_4 + 0.5 mol.% NiCl_2 + 1.0 mol.% H_2Asc (pH 4 and pH 6), with the current density varied over the 0.3-4.0 A/dm² range. Both the current efficiency of Fe-Ni alloy yield and the Ni content in the alloy were found to increase as the pH and the current density were raised, reaching 92 % and 57 % respectively (pH 6, 4.0 A/dm²). These data are based on total and partial cathodic polarization curves. Microstructural examination of the 70Fe-30Ni alloy in an electron diffractometer revealed a b.c.c. crystal lattice with $a = 0.286$ nm. Hardness tests revealed a greater microhardness of alloys with a higher Ni content, the microhardness of the 50Fe-50Ni alloy being 3.3 GPa. Figures 2; tables 3; references 2.

Model of Oriented Crystal Growth During Electrodeposition of Metals

917D0140F Moscow ZASHCHITA METALLOV
in Russian Vol 27 No 1, Jan 91 pp 157-162

[Article by N.V. Podbornov, A.I. Zhikharev, and I.G. Zhikhareva, Tyumen Industrial Institute]

UDC 541.137

[Abstract] A theory of preferential crystal orientation during electrodeposition of metal on same or other substrate metal is constructed in the form of a probabilistic model of crystal nucleation and subsequent layer-wise growth. The model is based on electrochemical

kinetics with an exponential dependence of the probability of crystal nucleation on the work of nucleation under given overvoltages, according to K. Vetter, and on the thermodynamics of subsequent crystal growth with a probability of preferential orientation generally dependent on four process parameters: overvoltage, reticular density, number of layers, and an attenuation coefficient representing the decrement of epitaxial influence of the substrate on successively deposited monolayers. Both probabilities have been calculated on the basis of this model for deposition of silver crystals (f.c.c. lattice) in 1-5 monolayers on platinum cathodes: with (111), (100) orientations on a Pt(100)-cathode under a 0.02 V overvoltage, with (111), (100), (110), (113) orientations on an isotropic Pt-cathode under a 0.02 V overvoltage, and with (111), (100), (110), (113), (210) orientations on both cathodes (the probability of other orientation being zero). An experiment involving pulsed potentiostatic electrodeposition of copper from sulfate solutions on isotropic platinum substrates has yielded data on the ranges of overvoltage for deposition of copper crystals (f.c.c. lattice) with [111], [100], [110], [113], [210] orientations on an isotropic platinum substrate, which agree quite closely those calculated on the basis of this model. Figures 1; tables 2; references 8.

Passivation of Chromium Steels During Isothermal Oxidation Under Low Oxygen Pressure

917FD0140D Moscow ZASHCHITA METALLOV
in Russian Vol 27 No 1, Jan 91 pp 49-54

[Article by Ye.K. Oshe, T.Yu. Zimina, T.Yu. Tabachnikova, M.N. Churayeva, L.V. Sapozhnikova, and P.A. Zimin, Institute of Physical Chemistry, USSR Academy of Sciences]

UDC 620.197.3

[Abstract] Two chromium steels for the electronic industry, ferritic 09Cr17Ti (0.09 %C, 16.99 Cr%, 0.53 %Mn, 0.03 %Si) and semiferritic 1Cr13 (0.112 %C, 12.94 %Cr, 0.5 %Mn, 0.07 %Si), were isothermally oxidized at 600°C temperature under an air pressure varied from 1 atm down to 0.132 Pa and the partial oxygen pressure thus varied from 0.1976 atm to 0.0264 Pa, for a study of their passivation under these conditions. Each oxidation treatment lasted for 2 h, whereupon specimens of these steels were cooled to room temperature in a furnace under a pressure of 26.4 mPa. The oxidation rate was measured in a "Gartner" L-119 XUV ellipsometer using 522 nm and 585 nm light incident at a 55° angle, for a determination of its dependence on the oxygen pressure. The phase composition of oxide surface layers was analyzed by the back-reflection method in an electron diffractometer with a $\text{Co}_{\text{K}\alpha}$ radiation source and a TiO_2 reference specimen, x-ray electron spectroscopy after 7-10 nm deep electrolytic etching was performed in a VGESCALABS-5 instrument with an $E_{\text{K}\alpha} = 14,866$ eV radiation source. The defective structure of oxide films

was examined by the photoelectric polarization method with a DRSh-250 flash lamp as source of square light pulses ($t_s/RC = 0.0025$, t_s - pulse duration, RC - time constant of photoelectric circuit). The electrical impedance at 50 Hz and 50 kHz frequencies in 1 N Na_2SO_4 was measured with a TESLA BM-507 meter on specimens with a 0.4 cm^2 surface area. The data indicate that the thickness of the oxide film on 09Cr17Ti steel peaks to its $d \approx 130 \text{ nm}$ maximum under a 0.264 Pa residual oxygen pressure, passivation occurring under higher pressures. Its thickness on 1Cr13 steel varied over the 80-130 nm range, but the reproducibility of data was poor so that its maximum could not be fixed. A surface film with n-type electrical conductivity was found to be forming on both steels during low-pressure hot oxidation. It consists of stable complex oxide $\alpha\text{-Fe}_2O_3\text{, Cr}_2O_3$, metastable complex oxide $\gamma\text{-Fe}_2O_3\text{, Cr}_2O_3$, manganese oxides, and their solid solutions. Figures 3; references 13.

Influence of Hydroxyl and Chromate Ions on Corrosion of Carbon Steel

917D0140B Moscow ZASHCHITA METALLOV
in Russian Vol 27 No 1, Jan 91 pp 33-39

[Article by V.P. Isupov, I.G. Gorichev, V.A. Shepontsev, and E.I. Rukin, Moscow State Pedagogical Institute imeni V.I. Lenin and Kirov State Pedagogical Institute imeni V.I. Lenin]

UDC 620.197.3

[Abstract] Corrosion tests were performed on grade-10 plain carbon steel for pulp, coal, and iron-ore pipe lines, their object being to evaluate the effectiveness of K_2CrO_4 as corrosion inhibitor. Its concentration was varied over the 0.05-5 mM range, natural water being simulated by a $1 \text{ g/dm}^3 Na_2SO_4 + 0.5 \text{ g/dm}^3 NaCl$ solution in pure water and its pH being regulated by addition of either H_2SO_4 or $NaOH$. All tests were performed either in phosphate buffer solutions (pH 7.0) or in support solutions with (pH 7.2) at $25 \pm 1^\circ\text{C}$ temperature. The corrosion rate ρ ($\text{g}/(\text{m}^2 \cdot \text{h})$) was determined from the loss of mass and from the polarization impedance, measurements being made on disk electrodes rotating at 500-1100 rpm under a partial pressure of oxygen (O_2) varied over the 0.01-0.21 atm range. Electric potentials were measured with a P-5827M potentiostat and polarization curves were plotted by the potentiodynamic method at a rate of 3 mV/s from the static potential on. Each test lasted for 6 h. The data indicate that the corrosion rate decreases as the oxygen pressure increases and as the pH is increased from 7.0 to 11, while the static potential increases as the oxygen pressure decreases but remains constant as the pH is up to 9.5 and then shifts in the positive direction as the pH is further increased. The polarization curves characterize dissolution of iron in 0.1 N Na_2SO_4 solution with the CrO_4^{2-} -ion concentration varied over the 0-1.0 g/dm^3 range. The experimental data indicate further how the anode

current, measured during potentiodynamic polarization (at 0.5 mV/s) of magnetite on a slowly rotating (500 rpm) disk electrode, depends on the CrO_4^{2-} -ion concentration and on the OH^- -ion concentration at a -200 mV potential. Theoretical calculations are based on empirical approximate relations for the static potential (multiple correlation coefficient $R = 1.000$, r.m.s. error $S = 0.5$ mV) and for the partial derivative of $\log \rho$ with respect to pH as well as on the Pleskov-Tarasevich model of cathodic oxygen ionization and the Lorenz-Miligy-Geana model of anodic iron (magnetite) dissolution-passivation involving hydroxyl ions. The results indicate that chromate ions do not significantly influence the anodic iron dissolution current and thus also not the second peak of the corresponding polarization curve, this peak being attributable to formation and growth of Fe_3O_4 spinel. Figures 4; tables 1; references 10.

Cathodic Behavior of TiC and of Carbide Surface Layers on Titanium

917D0140A Moscow ZASHCHITA METALLOV
in Russian Vol 27 No 1, Jan 91 pp 26-32

[Article by T.V. Chukalovskaya, N.P. Chebotareva, and N.D. Tomashov, Institute of Physical Chemistry, USSR Academy of Sciences]

UDC 620.198

[Abstract] An experimental study of sintered stoichiometric TiC and of carbide surface layers on Ti was made concerning their electrochemical characteristics and specifically anticorrosive properties. Carbide surface layers about 60 μm thick were deposited on Ti substrates by thermodiffusion impregnation of the latter with carbon black at 1100°C temperature in an Ar atmosphere for 5 h. These carbide layers as well as commercially pure VT1-0 and carburized Ti were tested electrochemically in a 5 N aqueous H_2SO_4 solution on a disk electrode rotating at a speed of 2020 rpm, at 30°C temperature in an Ar atmosphere. Cathodic polarization $e_H(\log i)$ curves were plotted by the potentiodynamic method at a rate of 2 mV/s and covered the $i = 0-3 \text{ A/m}^2$ range of current density, these curves showing carburized titanium to be intermediate between TiC and bare Ti with respect to cathodic protection effectiveness. The current density was measured over a 6 h long period and found to follow analogous trends on TiC and carburized Ti. On bare Ti at the same potential it was found to be much lower initially and then to increase slower, most likely because of TH_2 formation. Analysis of these data based on a review of all cathodic and anodic reactions on Ti and on TiC, taking into consideration their potentials, indicates that the TiC dissolves in 5 N H_2SO_4 at 30°C at an increasing rate as the cathode potential rises but remains more corrosion resistant than bare Ti at cathode potentials up to $e = -0.6 \text{ V}$. The cathodic process of hydrogen evolution becomes more intense with time, especially at high cathode potentials $e < -0.5 \text{ V}$. According to the

results of x-ray structural and phase analysis, thermodiffusion impregnation produces quite defective and highly nonstoichiometric $TiC_{0.5\ldots0.6}$ surface layers containing titanium oxides as inclusions. Cathodic polarization will therefore cause them to rapidly dissolve and disintegrate. Consequently, carburized titanium cannot provide corrosion protection in strong reducing media and is not a suitable material for a hydrogen-collecting cathode. Figures 3; references 15.

Formation of Titanium Coatings on Steel by Thermodiffusion From Melt

917D0141K Moscow ZASHCHITA METALLOV
in Russian Vol 27 No 2, Feb 91 pp 326-328

[Article by A.G. Sokolov, T.I. Ivanova, and A.V. Sivenkov, Leningrad Institute of Mechanics]

UDC 621.793.4.001.2.5:620.197.7

[Abstract] Titanium coatings were experimentally deposited on structural plain carbon steels (grades 3 and 45), on structural alloy steels (12Cr18Ni10Ti and 40Cr), and on tool steel (R-6Mo5) by thermodiffusion from a melt of Pb-Bi eutectic under vacuum. Cylindrical specimens 10 mm in diameter were thus coated in a SSHV-1,2.5/25-I1 vacuum furnace at temperatures ranging from 1100°C to 1250°C and with the process time regulated over the 2-20 h range. The coating deposition rate and the maximum coating thickness decrease with higher carbon content in the steel, an increasingly thicker hard and brittle TiC layer covering the carbon-free underlayer. The thickness of that underlayer increases as the duration of the process is lengthened. Successful titanium coating of medium-carbon and high-carbon steels requires that buildup of the TiC layer be inhibited, which can be done by coating these steels at temperatures higher than the carbide formation temperature. This possibility was demonstrated on R-6Mo5 steel: while only a 5 μm thick brittle carbide layer had formed in 10 h at 1200°C, a double-layer coating with a 20 μm thick carbon-free layer under a 10 μm carbide layer had formed in the same time at 1250°C. Figures 2; references 7.

Experience With Coating of Zinc Alloyed With Titanium

917D0141J Moscow ZASHCHITA METALLOV
in Russian Vol 27 No 2, Feb 91 pp 305-306

[Article by L.I. Kadaner and T.S. Bazilevich, Kharkov State Pedagogical Institute]

UDC 621.357.7

[Abstract] A nontoxic stable electrolyte has been developed at the Kharkov State Pedagogical Institute (KhGPI) for deposition of $Zn + (0.1\text{-}0.5) \text{ wt.\% Ti}$ coatings. This electrolyte consists of 2 g/dm^3 $Ti(SO_4)_2 \cdot 9H_2O + 40 g/dm^3 ZnSO_4 + 30 g/dm^3 (NH_4)_2SO_4 + 30 g/dm^3 Na_2SO_4 + 5 g/dm^3 NaCl + 8 g/dm^3$ KhGPI-1 additive + 1 g/dm^3 hide glue. The additive

forms with titanium a complex which is highly soluble in electrolytes with a pH ranging from 1 to 5. The range of deposition current density is 0.8-1.5 A/dm^2 , cathodic and anodic current efficiencies being balanced by use of Zn and graphite anodes. The electrolyte yields brilliant coatings of light color with strong adhesion and without pitting, 5-6 μm thick coatings of these alloys having a much higher corrosion resistance than 12-20 μm plain Zn coatings. Such coatings were tested, after chromizing in 25-30 $g/dm^3 Na_2Cr_2O_7 \cdot 2H_2O + 10-15 g/dm^3 Na_2SO_4$ solution. The deposition rate was 0.013-0.016 $g/(dm^2 \cdot min)$ with a current efficiency of 65-70 % at a current density of 1 A/dm^2 . The microhardness of these coatings is within the 1.5-2.0 GPa range, increasing with higher Ti content. Internal stresses in 4-6 μm thick coatings do not exceed 90 kPa, just as those in conventional Zn coatings. Coatings of $Zn + 0.3 \text{ wt.\% Ti}$ were tested in an MIM-1M machine and found to wear only 0.13-0.14 mg/dm^2 , as compared with a 0.36-0.37 mg/dm^2 of Zn coatings, over a 1000 m long path under dry friction. They were tested for corrosion with favorable results in aqueous 3 % NaCl solution, in gaseous SO_2 , in NH_3 vapor, in aqueous 5 % Na_2S solution, in a humidity chamber with and without condensation, and in open air (18 months in Kharkov hills), also in various agricultural enterprises including fertilizer plants. On the basis of these tests, typically 60 t of zinc for coating bolts and nuts in a tractor manufacturing plant can be replaced with 20 t of zinc and 100 kg of titanium.

Behavior of Ti-Nb-Ni Alloys in Sulfuric and Hydrochloric Acids

917D0141G Moscow ZASHCHITA METALLOV
in Russian Vol 27 No 2, Feb 91 pp 272-274

[Article by A.I. Shcherbakov, V.N. Dorofeyeva, N.D. Tomashov, B.A. Goncharenko, and V.S. Mikheyev, Institute of Physical Chemistry, USSR Academy of Sciences]

UDC 620.193.4

[Abstract] Titanium alloys of the Tb-Nb-Ni system with 0.2-2.0 wt.% Ni and 1-6 wt.% Nb were tested for corrosion and passivation in aqueous 5 N H_2O_4 and 5 N HCl solutions, pure titanium being known to dissolve vigorously in these acids. The alloys were produced in a lunate electric-arc furnace with a nonconsumable anode. Ingots were forged into rods about 10 mm in diameter, these being then annealed at 700°C for 1 h and furnace cooled. They were tested for the dependence of the corrosion rate on both alloying elements at 22°C over a 196 h (7 days) period and also at 60°C. Polarization curves were plotted potentiodynamically at the rate of 0.8 mV/s. The results indicate that increasing the total Ni and Nb content ennobles both corrosion and critical passivation potentials relative to a normal hydrogen electrode, without significantly changing the full-passivation

potential, and lowers the critical passivation current density. The results indicate that, while the electrochemical characteristics change monotonically with increasing Nb content, their dependence on the Ni content is not monotonic and increasing the Ni content above 2 wt.% does not further improve them. Addition of up to 2 wt.% Ni was found to raise the highest temperature at which the Ti + 8 wt.% Nb alloy would remain stably passive in 2 N H₂SO₄, but increasing the Ni content further up to 3 % did not raise that temperature further. As a cathodic passivating modifier, moreover, nickel was found to be more effective than niobium. Stable passivation of the Ti + 2 wt.% Ni alloy in 5 N H₂SO₄ at room temperature was found to require addition of at least 4 wt.% Nb, niobium influencing the anodic process much stronger than the cathodic process. The higher the Ni content in alloys with a Nb deficiency, the more readily they become active and the faster they dissolve. Passivation requires more than 1 wt.% Ni, and 2 wt.% will thus be the optimum Ni content. Figures 2; tables 2; references 5.

Emission Characteristics and Composition of Surface Layers of Fe-Si Alloys

917D0141E Moscow ZASHCHITA METALLOV
in Russian Vol 27 No 2, Feb 91 pp 263-266

[Article by N.V. Kolganova, N.G. Shirina, Yu.Ya. Tomashpol'skiy, V.I. Kolotyrkin, and V.M. Knyazheva, Scientific Research Institute of Physical Chemistry imeni L.Ya. Karpov]

UDC 620.193.4

[Abstract] An experimental study of Fe-Si alloys was made, for a determination of their electron emission characteristics depending on their composition. Five alloys of the Fe_{100-x}Si_x series with x = 12, 27, 38, 50, 67 (atom.%) respectively were tested, one series of specimens having been quenched at a rate of 10⁶°C/s and one series of specimens having been conventionally smelted without quenching. The latter specimens were polished to a mirror surface finish and then ultrasonically degreased in acetone. The composition of all specimens was monitored by x-ray microanalysis under a JSM-35 CF electron microscope with a LINK-860 attachment for x-ray spectrum analysis. Surface phase analysis based on diffraction of fast (100 keV) electrons was performed under a JEM- 100 CX electron. Electron emission by all these alloys was upon their bombardment with a beam of 5-25 keV electrons was tracked under a JSM-2 electron microscope. According to theory, the total electron flux coming from the surface of a solid body bombarded by fast (E ≥ 1 keV) electrons consists of secondary-emission electrons and inelastically scattered electrons, with slow (E ≤ 50 eV) electrons contributing about 90 % of that total flux. While secondary emission of electrons depends largely on the surface microstructure and the surface treatment, inelastic scattering of electrons depends largely on the composition of the about 100 nm thick surface layer. Secondary emission was measured

with the detector recording the total flux. Measurements of inelastic scattering were made with slow (E ≤ 50 eV) electrons were filtered out. The results indicate that the secondary electron emission increases slightly with increasing silicon content, this dependence on the alloy composition being monotonic for the quenched series. For the unquenched series this dependence is nonmonotonic with an anomaly, a high peak preceded by a dip and followed by a dip with maximum secondary electron emission by the Fe + 50 atom.% Si alloy. According to an analysis of reflection diffractograms, this anomaly may be attributable to the polishing of unquenched alloys. This surface treatment produces deformed surface layer and thus tends to generally weaken the subsequent secondary electron emission, but evidently has amorphized a thin surface layer on the Fe + 50 % Si alloy and thus enhanced the subsequent secondary electron emission. The diffractograms also indicate formation of Fe₇₃Si₂₇ and Fe₃Si phases on the surface of alloys up to 38 atom.% Si as a results of ultrafast quenching. Figures 2; references 5.

Tungsten Buildup on Surface of Ti-W Alloys

917D0141C Moscow ZASHCHITA METALLOV
in Russian Vol 27 No 2, Feb 91 pp 221-226

[Article by A.I. Shcherbakov, Institute of Physical Chemistry, USSR Academy of Sciences]

UDC 620.193.4

[Abstract] The buildup of tungsten on the surface of binary Ti-W alloys due to selective dissolution of titanium during cathodic polarization of these alloys is evaluated on the basis of an experimental study and a theoretical analysis of its results. Corrosion tests were performed on four "martensitic" Ti-W alloys containing 1, 3, 5, 10 wt.% W respectively, in an aqueous 5 N H₂SO₄ solution (de aerated with argon) at 30°C. Cathodic polarization curves were plotted galvanostatically with a PI-50-1 potentiostat, covering the range of potentials more positive than the standard -1.75 V titanium potential and more negative than the standard -0.09 V tungsten potential. Overvoltage and weight fraction of tungsten on the surface were measured as the cathode current density was varied stepwise in accordance with the electrochemical characteristics of the series, from 4.7 mA/m² for Ti-1W (3.3 mA/m² for 100 % Ti) to 75 mA/m² for Ti-10W (100 mA/m² for 100 % W). Theoretical calculation of the overvoltage is based on Tafel's equation, assuming an equipotential alloy surface and pure alloy components. With hydrogen evolving at the cathode, the dependence of the overvoltage on the logarithm of current density is linear only when the Tafel slopes β_{Ti} and β_W are equal. In this case Tafel's equation simplifies so that the overvoltage can be expressed as an explicit function of current density and tungsten weight fraction on the alloy surface, otherwise it can be calculated by the method of successive approximations. The results of these calculations indicate that the tungsten

surface atom.% increases as the tungsten volume atom.% increases. Overvoltages calculated on the basis of the tungsten volume atom.% are found to be higher than the measured overvoltages. The tungsten surface atom.% subsequently calculated on the basis of overvoltage measurements are then found to be higher than the tungsten volume atom.%, which indicates an excess of tungsten on the alloy surface. Such a buildup of tungsten on the alloy surface is mathematically described by the equation of solid-state diffusion kinetics with a moving front. An asymptotic solution of this equation for given initial and boundary conditions, with the aid of Laplace integral transformations, yields the W-concentration on the alloy surface as a function time with both Biot and Tikhonov numbers for titanium as dimensionless parameters. While theoretically the final Ti-concentration on the alloy surface should be zero at time $t \rightarrow \infty$, in the experiment there was always reached a steady state of balance between diffusion of tungsten and dissolution of titanium with the diffusion front moving so that the thickness of the diffusion layer remained constant. Figures 3; tables 1; references 10.

Function Describing Change of Rate of Air Corrosion of Metals in Time. Effect of Atmospheric Conditions and of Alloying Elements on Corrosion Resistance of Steels and Cast Irons

917D0141D Moscow ZASHCHITA METALLOV
in Russian Vol 27 No 2, Feb 91 pp 248-262

[Vu Din Vuy, Vietnam National Center of Scientific Research, Hanoi Institute of Tropical-Climate Technology, Institute of Physical Chemistry at USSR Academy of Sciences]

UDC 620.193.2

[Abstract] Experimental data on air corrosion of 59 types of cast irons, plain carbon steels, and low-alloy steels tested in 49 regions of the world have been processed on an Iskra-226 microcomputer using standard computer programs, in accordance with the author's function of time (ZASHCHITA METALLOV, Vol 26 No 6, 1990) $K = K_0/(1 + \alpha_0 t) = K_1/(C_1 + \alpha_1 t)$ (K - average rate of air corrosion at any instant to time t prior to stabilization $\mu\text{m}/\text{yr}$ or $\text{g}/\text{m}^2\text{.yr}$, K_0 - initial rate of air corrosion, K_1 - known rate of air corrosion at instant of time t_1 , $K_1/K = C_1 + \alpha_1 t$, α_0 , α_1 - passivation coefficients representing the protective passivating action of corrosion products from time t_1 to time t and from time $t = 0$ to time t respectively). The purpose was to determine on the basis of statistical analysis how the initial corrosion rate K_0 at the active surface, the protective effect of passivation by corrosion products α_0 , and the resistance to air corrosion $g\alpha_0/K_0$ depend on the atmospheric conditions and on the alloying elements. The data for this evaluation, covering periods of 1 to 3, 7, 12 years and coming from test stations in several countries (USSR, Norway, Czechoslovakia, USA, Panama, Brazil), represent four types of environment (rural, urban, maritime, industrial) in a

wide range of climates (subarctic, temperate, subtropical with dry air and subtropical with humid air, tropical). Some of the general conclusions based on the analysis of these data are that the initial corrosion at the active surface of all these ferrous materials is lowest in rural air and highest in industrial air, that the protective effect of passivation by corrosion products is strongest in industrial air weakest in maritime air, that the corrosion resistance of all these ferrous materials is highest in rural air and lowest in maritime air, that Cu, Ni, Si, Cr increase the corrosion resistance of steel in maritime air much less than the corrosion resistance in other air, that Mn increases the corrosion resistance of steel in maritime air much more than do the other alloying elements, that V as another alloying element improves the protective passivating action of corrosion products in rural, urban, and industrial air. The author thanks Professor Yu.N. Mikhaylovskiy and Senior Scientific Associate P.V. Strekalov for helpful discussions of the results. Tables 8; references 17.

Effect of Polarization on Development of Ocean Bacteria During Galvanic Corrosion of Metals

917D0141I Moscow ZASHCHITA METALLOV
in Russian Vol 27 No 2, Feb 91 pp 286-292

[Article by Yu.M. Korovin and A.V. Ledenev, Institute of Oceanography imeni P.P. Shirshov, Southern Department, USSR Academy of Sciences]

UDC 541.144.7

[Abstract] The effect of anodic and cathodic polarization on the development of ocean bacteria on metals during galvanic corrosion under natural conditions is analyzed on the basis of 600 h (25 days) long tests performed 1.5-5,000 m deep in the Atlantic Ocean. Measurements were made on the surface of 4sp killed low-carbon steel in four galvanic pairs with L-63 brass, M-1 copper, Cr18Ni10Ti stainless steel, and 3M Al-Mg alloy respectively. Along with the corrosion rate were measured the total bacterial overgrowth as well as development of saprophytes, ammonifiers, and sulfate-reducing bacteria separately each, the current density varying depthwise over the 0.5-1.5 A/m² range (0.5-0.8 A/m² across 4sp/Cr18Ni10Ti contact, 0.6-1.0 A/m² across 4sp/3M contact, 0.8-1.5 A/m² across 4sp/L-63 and 4sp/M-1 contact). On the basis of these data have been calculated two numerical ratios (number of bacteria on plate with polarization to number of bacteria on same plate without polarization), γ_{an} characterizing the behavior of microorganisms on the surface of anodic 4sp steel and γ characterizing their behavior on the surface of cathodic L-63, M-1. The results indicate that anodic polarization stimulates overall development of bacteria and that cathodic polarization either inhibits or does not influence it, with the exception of stimulating development of ammonifiers on copper, brass, and stainless steel. Anodic polarization stimulates particularly development of saprophytes on carbon steel. On anodically polarized

aluminum alloy the behavior of ammonifiers is found to be similar to the behavior of saprophytes, their development being quite intense. Anodic and cathodic polarization due to corrosion suppresses biochemical activity of ammonifiers. Development of sulfate-reducing bacteria is found to vary depthwise almost equally on all four galvanic pairs. It is noted that the increase of γ_{an} with depth is attributable not to the increasing current density but to the decreasing total number of bacteria on non-polarized plates as well as on polarized ones. Figures 2; tables 3; references 4.

Electrochemical Behavior and Corrosion of Stainless Steels in Model Solutions of Nutrient Salts Simulating Production of Food Protein From Natural Gas

917D0140C Moscow ZASHCHITA METALLOV
in Russian Vol 27 No 1, Jan 91 pp 44-48

[Article by Yu.S. Ruskol and L.I. Viter, Scientific-Industrial Association "Biotehnika" (Bioengineering)]

UDC 620.193.41

[Abstract] Eight stainless steels (08Cr17Ti, 06CrNi18MoCuTi, 08Cr17Ti, 10Cr17Ni13Mo2Ti, 08Cr18Mn8Ni2Ti, 12Cr18Ni10Ti, 08Cr21Ni6Mo2Ti, 08Cr22Ni6Ti), grade-3 pure carbon steel, and BT1-0 commercially pure titanium were tested for corrosion in aqueous solutions of five salts (7.00 g/dm³ and 0.60 g/dm³ KCl, 8.14 g/dm³ and 7.43 g/dm³ K₂SO₄, 6.00 g/dm³ MgSO₄, 0.80 g/dm³ FeSO₄, 0.75 g/dm³ CuSO₄) and one acid (20.0 g/dm³ H₃PO₄) at 45°C temperature, simulating conditions of food protein production with use of methane as source of carbon for microbiological synthesis. The water was distilled, chemically pure or analytically pure. All solutions had a pH within the 1.75-1.9 range and were naturally aerated. River or circulating water was simulated by the 7.43 g/dm³ KCl solution. The test specimens were 2-5 mm thick rectangular bars and 2-5 mm thick welded joints with a transverse seam in the middle. Laboratory tests lasted 1000 h each and industrial tests lasted 6500 h each. Dissolution curves were plotted potentiodynamically at a rate of 1.8 V/h in a standard three-electrode cell. The pitting potential and the pitting repassivation potential, relative to a normal hydrogen electrode, were measured by the Freyman-Flis-Prazhak method (L.I. Freyman, Ya. Flis, M. Prazhak, et al., ZASHCHITA METALLOV Vol 22 No 2, 1986), the pitting depth being measured under an MMR microscope (Leningrad Association for Mechanics and Optics). Additional tests were performed in 7 g/dm³ KCl solutions with the pH lowered to 1.70 by addition of various acids (HCl, H₂SO₄, H₃PO₄). The results of this study indicate that all these steels, except grade-3 plain carbon steel and 15Cr25Ti chromium steel, have a high resistance to pitting and general corrosion. Two steels, 12Cr18Ni10Ti and 08Cr22Ni6Ti, were found to remain passive over a wide range of potentials and, therefore, to be almost completely immune to pitting in

those solutions (7.43 g/dm³ KCl) under real conditions. Figures 3; tables 2; references 10.

Corrosion Resistance of 02Cr8Ni22Si6 (EP794) Low-Carbon Alloy Steel

917D0193B Moscow TYAZHELOYE
MASHINOSTROYENIYE in Russian No 5, May 91
p 33

[Article by N.A. Adugina, candidate of technical sciences, L.A. Andreyeva, V.M. Alekseyeva, Yu.A. Tsyganov, and G.A. Zheltova, Scientific Research Institute of Chemical Apparatus]

UDC 620.193:669.15-194

[Abstract] A special low-carbon high-silicon alloy steel has been developed jointly by the Central Scientific Research Institute of Ferrous Metallurgy and the State Scientific Research and Planning Institute of the Nitrogen Industry for equipment used in production of 98 % HNO₃ concentrate, this austenitic 02Cr8Ni22Si6 (EP794) steel (7.5-10 % Cr, 21-23 % Ni, 5.4-6.7 % Si) containing less than 0.3 % C and up to 0.20 % residual Ti. Strip of this steel produced by hot rolling contains less than 0.02 % C and only scarce silicide inclusions in a purely austenitic structure. So far weldments of this steel have been found to be subject to intense intercrystalline corrosion within the heat-affected zone and also to knife-line attack in boiling 98 % HNO₃ solution. The results of metallographic tests and examination indicate that the steel becomes prone to these form of corrosion after having been heated to temperatures within the perilous 600-700°C range during the welding process, knife-line attack being caused by subsequent precipitation of titanium carbides along the fusion line. Lowering the carbon content down to the 0.016 % C solubility limit does not fully inhibit intercrystalline corrosion but only confines it to smaller penetration depths and smaller regions within the heat-affected zone, owing largely to the high nickel content responsible for further lowering the solubility limit for carbon so that secondary carbides precipitate along grain boundaries. Stabilization of the steel increases its resistance to intercrystalline corrosion, niobium being a more effective stabilizer than zirconium or titanium, but it also decreases its plasticity by causing precipitation of the brittle silicide phase. Quenching from 1050°C in water is by far the best way to fully inhibit intercrystalline corrosion of 02Cr8Ni22Si6 steel weldments, inasmuch as the secondary phase dissolves. This is demonstrated by equipment which has been in service for four years already. At the same time, however, the steel and its weldments, whether quenched or not, are highly sensitive to a decrease of the HNO₃ concentration. This sensitivity, manifested in an appreciable increase of the corrosion rate, is attributable to the low chromium content. Only in 95-98 % HNO₃ concentrates does quenched steel have an adequately high adequately high resistance to general and intercrystalline corrosion at the boiling temperature, with a rate of

general corrosion not higher than 0.1 mm/yr. It is not suitable for holding less concentrated HNO_3 solutions.

Corrosion-Resistant Chromium Steel Without Nickel and Its Industrial Status

917D0193A Moscow TYAZHELOYE
MASHINOSTROYENIYE in Russian No 5, May 91
pp 26-28

[Article by V.P. Borisov, candidate of technical sciences, M.F. Vorokhanova, and N.A. Karpova, Scientific-Industrial Association: Central Scientific Research Institute of Heavy Machinery]

UDC 669.14.018.588.8

[Abstract] An economical corrosion-resistant alloy steel which contains no nickel has been developed for use in nuclear power and thermal electric power plant equipment. This wrought 08Cr14MoV chromium steel is certified for industrial production of strip and tubes, by hot rolling and cold forming respectively. The steel is smelted in an electric-arc furnace, which may be followed by vacuum-induction, vacuum-arc, or electroslag remelting. Hot forming should be done at temperatures within the 750-1250°C range. The steel belongs in the martensitic-ferritic class, consisting of sorbite and ferrite after it has been tempered. Its mechanical properties can be controlled by heat treatment. It remains corrosion-resistant in air, water, steam, and deactivating solutions at temperatures up to 500°C. After high-temperature tempering, moreover, it becomes also resistant to crevice corrosion by fluids with chloride content. Heat treatment in an oxidizing atmosphere first and then in a reducing atmosphere decreases uniform corrosion to 12.0 g/m²·h or less and inhibits pitting by deactivator fluids. Intercrystalline corrosion is inhibited by tempering at temperatures within the 680-760°C range and subsequent aging at 350°C for 3000 h. Corrosion of the 08Cr14MoV steel in mixtures of concentrated lactic acid with disinfectant and detergent solutions is uniform and proceeds at about the same rate as does corrosion of the austenitic 08Cr18Ni10Ti steel in such media. Its resistance to air corrosion in the industrial atmosphere of the eleventh climatic zone is very high. The thermal conductivity of the 08Cr14MoV steel is higher than that of Cr-Ni steels, which contributes to a much better heat transfer at the surfaces of apparatus made of this steel. The steel is also much less prone to strain hardening than are austenitic steels, which allows cold bending with up to 30 % deformation. The steel is weldable: parts made of it can be joined to one another and to parts made of another stainless steel or of a carbon steel by automatic welding under a flux or by manual arc welding with two electrodes, also by automatic or manual welding with a nonconsumable electrode and a filler. Over a hundred new heat exchangers for twelve nuclear and thermal electric power plants have been constructed with the new 08Cr14MoV steel. Use of this steel instead of the

08Cr18Ni10Ti steel for equipment in RBMK water-cooled graphite-moderated high-power channel reactors and VVER water-cooled water-moderated power reactors should reduce the cost by over 3 million rubles and save over 1000 tons of nickel (100 kg Ni per ton of metal). Use of this steel instead of copper alloys for steam generator tubing in nuclear power plants should improve the equipment by minimizing corrosion and scale formation. Tables 3.

Corrosion Resistance of High-Strength Cast Iron at High Temperatures in Oil Bed Water

917D0141H Moscow ZASHCHITA METALLOV
in Russian Vol 27 No 2, Feb 91 pp 283-286

[Article by Yu.A. Ishchuk, L.A. Solntsev, V.D. Shifrin, R.D. Dzhabarov, Kh.T. Kakhramanov, N.S. Fataliyev, and O.Yu. Rafiyev, Azerbaijan Planning and Design Institute of Petrochemical Apparatus Engineering]

UDC 669.131.7:620.193

[Abstract] The corrosion resistance of high-strength cast iron (ferritic grade VCh40, ferritic-pearlitic grade VCh50, pearlitic grade VCh60 in oil bed water and in superheated water vapor is evaluated, relative to that of 40Cr steel, on the basis of a planned experiment and a regression analysis. Specimens of each cast iron and of steel, 3 mm thick washers 30 mm in diameter, were tested in highly corrosive water simulating oil bed water and containing 95,968 mg/dm³ [Cl⁻], 465 mg/dm³ [HCO₃⁻], 595 mg/dm³ [SO₄²⁻], 5,914 mg/dm³ [Ca²⁺], 3,572 mg/dm³ [Mg²⁺], and 44,290 mg/dm³ [Na⁺] + [K⁺]. Tests were performed with and without stirring the water, the washers not touching one another nor the vessel walls in each case. The mathematical plan of the experiment was an asymmetric second-order 3-factorial (2-factorial for steel) 3-level one. Testing time, temperature of the medium, and Brinell hardness of the iron matrix were varied as follows: lower level (24 h without stirring, 6 h with stirring, 20°C, 175 HB) - middle level (192 h without stirring, 24 h with stirring, 50°C, 225 HB) - upper level (360 h without stirring, 42 h with stirring, 80°C, 275 HB). The target parameter, to be minimized, is the corrosion rate. The results indicate that stirring the water slows down the corrosion of each cast iron, more after longer exposure time, most effectively the corrosion of pearlitic cast iron (VCh60) and least effectively the corrosion of ferritic cast iron (VCh40), but hardly at all the corrosion of chromium steel. They also indicate that raising the water temperature lowers most appreciably the corrosion resistance of pearlitic cast iron (VCh60), chromium steel being least sensitive to temperature change. After a period of 360 h at 80°C, VCh60 cast iron already corroded slightly slower than and VCh40 cast iron corroded almost as slow as 40Cr steel. In stirred water the corrosion rate of 40Cr steel was found to dip to

a minimum after 24 h and to increase again during longer exposure to rates higher than the corrosion rate of cast iron, its sensitivity to temperature change in stirred water being approximately the same as that of the corrosion rate of VCh50 cast iron. During additional tests in wet water vapor at temperatures up to 200°C under a pressure of 1.6 MPa the corrosion rate of ferritic cast iron (VCh40) was about twice as high as that of pearlitic cast iron (VCh60) and 1.4-1.5 times higher than that of 40Cr chromium steel. According to the results of this study, low-alloy chromium steel in petrochemical apparatus may be replaced with high-strength cast iron containing globular graphite. Tables 2; references 3.

Dependence of Electrochemical Behavior and Corrosion Characteristics of $(Fe,Cr)_{85}B_{15}$ Alloys on Cr Content

*917D0141F Moscow ZASHCHITA METALLOV
in Russian Vol 27 No 2, Feb 91 pp 267-268*

[Article by G.V. Borisova, V.V. Maslov, D.Yu. Paderno, and S.S. Pustinnikov, Institute of Metal Physics at UkrSSR Academy of Sciences and Dnepropetrovsk Industrial Institute]

UDC 620.193.4

[Abstract] Four amorphous $Fe_{85-x}Cr_xB_{15}$ alloys with $x = 4.25, 8.5, 12.75, 17.0$ (atom.%) respectively were tested for electrochemical behavior and corrosion in an aqueous 3 % NaCl solution simulating sea water, 0.022-0.030 mm thick and 12-20 mm wide ribbons for this study having been produced by quenching jets of molten alloy. Microstructural examination in an x-ray diffractometer with a MoK_{α} -radiation source revealed no significant effect of chromium on their atomic structure. The corrosion rate was measured by the weighing method, corrosion products being removed with an aqueous 20 % $HCl + 0.8\% PB-5$ inhibitor solution. Anodic polarization curves were plotted with a P5827M potentiostat in a standard electrochemical cell, the potential relative to a $AgCl$ saturation electrode being raised in 50 mV steps and held at each level for a 120 s long period. The results indicate that the corrosion potentials of these alloys in sea water are comparable with those of 12Cr13 and 12Cr17 chromium steels and that their chemical stability also increases with increasing Cr content. The alloys with up to 5 atom. % Cr do not become passivated in 3 % NaCl solution, while those with 8.5 atom. % and higher Cr content are exceedingly susceptible to passivation. As the Cr content increases from 8.5 atom. % to 17 atom. %, the anode current density in the passive state decreases by an order of magnitude and the passivity range extends to the oxygen evolution potential. Only the alloy with 17 atom. % Cr was found to be immune to pitting, up to overpassivation at $\phi \geq 1.4$ V potentials. Figures 2; references 9.

Corrosion Characteristics of Grade-45 Carbon Steel Chromized and Chromosilicized by Diffusion Process in Protective Media

*917D0141B Moscow ZASHCHITA METALLOV
in Russian Vol 27 No 2, Feb 91 pp 202-208*

[Article by O.V. Kasparova, A.A. Zorin, Ya.M. Kolotyrkin, L.A. Gnezdilova, and S.V. Kostromina, Scientific Research Institute of Physical Chemistry imeni L.Ya. Karpov]

UDC 620.193.4

[Abstract] A comparative corrosion study of grade-45 carbon steel chromized and chromosilicized by diffusion impregnation was made, for a comparative evaluation of these treatments in a protective medium, without a protective medium, and under vacuum. Each treatment was followed by corrosion tests in aqueous 5 % H_2O_4 , 98 % H_2SO_4 , 27-98 % HNO_3 , and 3 % NaCl solutions at 40°C and at 90°C in each, for 240 h in H_2SO_4 and NaCl solutions, for 960 h in HNO_3 solutions. Overall corrosion rates as well as partial iron and chromium corrosion rates were measured throughout the test period, readings taken after 96 h during the 240 h tests and after 288 h during the 960 h tests serving as key trend indicators. The depthwise distributions of iron, chromium, and silicon concentrations in the surface layers were determined on the basis of x-ray analysis by the energy dissipation method. The results indicate that chromizing and chromosilicizing in an argon atmosphere, also chromizing under vacuum, increases the corrosion resistance of grade-45 carbon steel in these media by minimizing the porosity of the protective surface layer. Activation analysis has moreover revealed that chromizing this steel under vacuum is particularly effective in lowering the rate of iron corrosion in 5 % and 98 % H_2SO_4 solutions, also that chromizing the steel in an argon atmosphere inhibits its corrosion in 98 % H_2SO_4 and 3 % NaCl solutions much more effectively than does chromosilicizing it in an argon atmosphere. Figures 4; tables 2; references 7.

Capabilities of High-Energy Surface Treatment Methods for Corrosion Protection of Metals

*917D0141A Moscow ZASHCHITA METALLOV
in Russian Vol 27 No 2, Feb 91 pp 179-196*

[Article by V.I. Kolotyrkin and V.M. Knyazheva, Scientific Research Institute of Physical Chemistry imeni L.Ya. Karpov]

UDC 620.193.4

[Abstract] Four known methods of surface treatment for corrosion protection of metals are overviewed and comparatively evaluated on the basis of the state of the art worldwide. Plasma(H_2, N_2, Ar , $Ar+N_2$)-arc deposition of coatings features high particle temperatures and velocities ensuring formation of very tight coatings of all

refractory materials. Its advantages include high productivity, owing to a high heat transfer coefficient, moderate heating of the base material (metals, ceramics, graphite, thermoplastics) not beyond safe 100-200°C temperatures, flexibility which allows deposition of multilayer, pack, and composite coatings, easy process control, and mobility of equipment, also adaptability to almost any size and shape of coated surfaces. Detonation gas-flame spraying features ultrahigh particle energy ensuring very tight coatings with a strong adhesive bond to the base metal. It is workable with practically all coating materials, also unconventional ones such those with a high nonmetallic content. It is eminently suitable for deposition of highly wear-resistant and corrosion-resistant thick coatings on surfaces of almost all sizes, typically on inside surfaces of pipes. Under severe conditions such as on sea vessels these coating provide a better corrosion protection than do coatings deposited by the plasma-arc method. Laser treatment of metal surfaces offers the advantages of highly localized contactless heating without warpage, high speed and high productivity, access to remote or otherwise inaccessible targets, and fitness for automation. Most commonly in use are pulsed or continuous-wave gas lasers (CO_2) and solid-state lasers (ruby). Possible forms of laser treatment for corrosion protection are surface hardening without melting but with hardfacing, surface remelting for homogenization, hardfacing for structure modification, including amorphization, surface alloying, surface plating, and hardfacing of coatings for reduction of their porosity. Electron-beam treatment of metal surfaces offers the advantages of inhibiting equilibrium phase transformations and, therefore ensuring fixation as well as more uniform distribution of high-temperature phases over the surface layer. It homogenizes the surface layer chemically by more uniformly distributing all principal and impurity elements, it prevents or at least retards intercrystalline segregation of impurities, it prevents intergranular corrosion by dissolving carbides and liquefying boundary layers depleted of corrosion-resistant components, it facilitates transition of the surface layer to a microcrystalline or amorphous state in the melting and quenching process, thus minimizing the number of active corrosion-prone centers. Electron-beam treatment is also suitable for surface alloying and for reducing the porosity of protective coatings by their hardfacing. Each of these four methods has its also drawbacks and may be the best one for specific applications only. Figures 7; tables 3; references 157, including 15 available since March 1989.

Increasing Rail Protection From Electrocorrosion

917D0181A Moscow ELEKTRICHESKAYA I
TEPLOVOZNAYA TYAGA in Russian No 5 (413),
May 91 pp 43-45

[Article by A.V. Naumov, All-Union Scientific Research Institute of Railway Transport]

UDC 625.143.3:620.197.3:624.19

[Abstract] Methods of protecting rails and rail fasteners in DC sections of tunnels by means of rectifier sectioning

are summarized. Block-diagrams of rail circuit rectifier sectioning (VSRS) and rail circuit sectioning rectifier units (VBSRS-1) are presented; the VSRS was developed and built on the basis of a Railway Transport Institute project in the framework of the Manual to protect underground railway structures from stray current-induced corrosion (TsE-3551). The design was dictated by the results of a survey of 24 tunnels which revealed that even though the train stays no more than 3-4 min inside a tunnel of a 1-2 km mean length, which makes up only 6-10% of the day for all trains, the potential on the rail and, consequently, leakage from the rail linger much longer - up to 70% of the time. The use of protection systems makes it possible to decrease the rail potential by four to sixfold. The shortcomings of some systems, primarily due to the damage to thyristors and diodes in the units, and the causes of their failure are analyzed. Various studies helped to establish an optimal VSRS device maintenance schedule. They show that to ensure normal VSRS functioning, all elements and units must be comprehensively checked and inspected at least twice a year, preferably in April-June and October-December. Figures 3; tables 1.

Surface Titanium Alloying (Modification) by Laser Irradiation

917D0189B Moscow ZASHCHITA METALLOV
in Russian Vol 27 No 3, May-Jun 91 pp 467-471

[Article by N.D. Tomashov, I.B. Skvortsova, V.S. Mezhevov, I.V. Bobkov, R.Kh. Zalavutdinov, Physical Chemistry Institute at the USSR Academy of Sciences]

UDC 620.193.01

[Abstract] Electrochemical properties of surface-doped alloys produced by various methods, such as plasma and electrospark alloying, etc., are investigated. In particular, the possibility of developing Ti-Ni surface alloys on titanium by laser irradiation of a titanium surface covered with a nickel layer beforehand is examined. It is shown that during such treatment, rapid surface heating with subsequent quick cooling (due to a heat dissipation inward) may lead to the development of a surface alloy with a high structure disordering degree approaching the amorphous state. Experiments were carried out in a unit with a LTN-103 commercial CO_2 YAG CW laser. The alloying element was added by a coating containing 50% (by mass) nickel powder. Electrochemical characteristics of the laser-treated samples and, for comparison, pure nickel, titanium, and Ti_2Ni intermetallic were determined in a 0.5M NaCl solution. An analysis of experimental results demonstrates that in principle, it is possible to develop Ti-Ni surface alloys on a titanium base by the above method. Surface alloying can be optimized and sufficiently thick Ti-Ni coats with a good bonding to the base can be produced by manipulating the laser radiation power. The electrochemical properties of surface layers made under optimal laser treatment conditions are close to those of the Ti_2Ni intermetallic which

is characterized by a high passive state stability and efficiency for chlorine separation on the anode. References 7: 6 Russian, 1 Western; figures 3.

On Conjoint Effect of Silicon and Carbon on Intercrystalline Corrosion in Tempered Austenite Stainless Steels in Highly Oxidizing Media
917D0189A Moscow ZASHCHITA METALLOV in Russian Vol 27 No 3, May-Jun 91 pp 355-361

[Article by O.V. Kasparova, V.M. Milman, Ya.M. Koltynkin, Physicochemical Scientific Research Institute imeni L.Ya. Karpov]

UDC 620.193.01

[Abstract] The effect of silicon on intercrystalline corrosion (MKK) of Kh20N20 tempered austenite steel with varying carbon concentrations in highly oxidizing

media, i.e., potentials which correspond to the repassivation area, is considered. Sheet samples of Kh20N20 steel were quenched at 1,100°C in water and then tempered at 650° for 1, 10, and 100 h and 800° for 10 h. Then the samples were tested in boiling solutions of 27% HNO₃ containing 4 or 40 g/l of Cr⁶⁺ using 2-4 24-hour cycles. The mean corrosion rate was measured by the mass lost in each test cycle. An analysis of experimental data demonstrates a synergism of negative effects of carbon and alloying additions of silicon on the intercrystalline corrosion resistance of tempered austenite stainless steels at a potential which corresponds to the repassivation energy. It is also shown that this phenomenon is manifested only in the presence of chromium-depleted zones along the grain boundaries and is largely due to a degradation of these zones' resistance under the effect of silicon additions. References 15: 10 Russian, 5 Western; figures 4; tables 1.

Rolling Steel Strip With Continuous Heating

917D0142A Kiev PROBLEMY SPETSIALNOY ELEKTROMETALLURGII in Russian No 1, Jan-Mar 91 pp 38-43

[Article by B.Ye. Paton, B.I. Medovar, B.I. Shukstulskiy, L.B. Medovar, and M.V. Rymarchuk, Institute of Electric Welding imeni Ye.O. Paton, UkrSSR Academy of Sciences, Kiev]

UDC 669.187.56.002.5

[Abstract] Hot rolling of wide steel strip in the "Steckel mill", a four-high mill with small rolls, is being reconsidered in the United States and in Germany following the latest trend from large-scale production in giant plants to small-scale production in miniplants. The main advantages of this mill, a reversing mill with full power applied as forward and back tension, are precise temperature control and high product quality in terms of uniform sheet thickness. The mill, which had become almost obsolete, is being modified for current requirements which include full automation. New plants are being designed and old plants are being redesigned so that continuous casting and subsequent hot rolling in the Steckel mill can be combined for maximum technological efficiency and maximum economy of "compact" steel strip production. Only three old reversing mills are operating in the USSR. It would be advisable that in the USSR, too, introduction of the modernized Steckel mill be given serious consideration in production planning for the year 2000. Figures 2; references 9.

Production Line USh-172 for Large-Scale Electroslag Chill Casting of Slabs From Liquid Charge

917D0142B Kiev PROBLEMY SPETSIALNOY ELEKTROMETALLURGII in Russian No 1, Jan-Mar 91 pp 43-45

[Article by Yu.V. Orlovskiy, V.Ya. Maydannik, G.B. Shchupak, A.D. Chepurnoy, and Yu.N. Demchenko, Institute of Electric Welding imeni Ye.O. Paton at UkrSSR Academy of Sciences, Kiev, and Scientific-Industrial Association "Azovstal" (Azov Steel), Mariupol]

UDC 669.187.56.002.2

[Abstract] A production line for electroslag chill casting of slabs from liquid charge has been developed jointly by "Azovstal" and the Institute of Electric Welding, slabs weighing up to 2 tons being produced by this USh-172 line at a rate of 30,000-50,000 tons annually. The line includes two sets of crucible, gas heater, and chill. Each chill is mounted on a tilting cradle made to abut against the crucible, the gas heater for each crucible being mounted cantilever-wise on a transfer trolley carrying the chill. There is also included a common filter for unloading slab ingots. The production cycle consist of 11

operations. The line is technologically most advanced, slabs of top quality being produced here most economically. Figures 2.

Phase Formation in Vacuum Condensates of Binary Oxides With Titanium Oxide

917D0142C Kiev PROBLEMY SPETSIALNOY ELEKTROMETALLURGII in Russian No 1, Jan-Mar 91 pp 56-59

[Article by V.D. Kushkov, A.M. Zaslavskiy, I.S. Kozlov, A.V. Melnikov, and A.E. Slivinskaya, Kiev State University imeni T.G. Shevchenko]

UDC 669.187.526.001.5

[Abstract] An experimental study of vacuum condensates of binary oxides TiO_2 - M_2O_3 ($M = Al, Y, La$) with a wide range of the M_2O_3 fraction was made, its purpose being to determine the optimum conditions for formation of titanates. Condensates were vacuum-deposited on polycrystalline molybdenum substrates from vapors of two oxides, to a thickness of about 100 μm , following electron-beam vaporization of annealed compacts of extra-pure Al_2O_3 , Y_2O_3 , La_2O_3 , and TiO_2 powders in a separate crucible each. The substrate temperature was varied over the 500-1300°C range in 100°C steps. The phase composition of condensates was determined in a DRON-3 x-ray diffractometer with a CuK_α -radiation source, covering the 10-120° angles. Their chemical composition was determined on the basis of x-ray spectrum microanalysis in a REM-200 instrument with use of metallic Al, Y, La, Ti as references and with use of the "Karat" program for processing primary data. Aluminum titanate Al_2TiO_5 was found to form only on substrates at 1200-1300°C temperatures, with an only narrow 2 wt.% Al_2O_3 range of homogeneity and otherwise coexisting with rutile when the Al_2O_3 fraction deviates more than 2 wt.% from the equimolar one. Yttrium titanate Y_2 was found to form on substrates at all temperatures: coexisting with rutile at low temperatures, with rutile and anatase at 700-800°C, and with a solid solution which has a fluoritic structure when Y_2O_3 exceeds 32 wt.% (up to 45 wt.% at 500°C, 65 wt.% at 1300°C). Three lanthanum titanates were found to form: $La_2Ti_2O_7$, with a 30-45 wt.% La_2O_3 range of homogeneity and La_2TiO_5 with a 52-60 wt.% La_2O_3 range of homogeneity at temperatures not exceeding 1000°C, $La_4Ti_9O_{24}$ with no range of homogeneity only coexisting with one of other or with both other phases. Figures 3; references 7.

Feasibility of Using Ceramic Filters for Refining Stainless Steel With Titanium Content

917D0142D Kiev PROBLEMY SPETSIALNOY ELEKTROMETALLURGII in Russian No 1, Jan-Mar 91 pp 81-83

[Article by M.V. Rymarchuk, B.I. Shukstulskiy, L.B. Medovar, V.Ya. Sayenko, A.D. Chepurnoy, and A.V.

Litvinenko, Institute of Electric Welding imeni Ye.O. Paton at UkrSSR Academy of Sciences, Kiev, and Scientific-Industrial Association "Azovstal" (Azov Steel), Mariupol]

UDC 669.187.65.001.5

[Abstract] An experimental study was made at an "Azovmash" steelmaking plant concerning removal of titanium nitrides and carbonitrides from the molten metal prior to casting by means of foam ceramic filters, removal of these inclusions being necessary on account of their detrimental effect on the plasticity characteristics and the grindability of stainless steel. The effectiveness of such filters was tested in a 5-ton acid electric-arc steel melting furnace for production of 12Cr18Ni10Ti steel, molten metal being poured through an intermediate ladle simultaneously into two 1-ton strip molds. In

the drag of each mold had been installed a vertical barrier made of a refractory material with perforations, ceramic filters being placed in one of them and the holes in the other being partly covered so as equalize the hydrodynamic resistance of both. The filters, made of $\text{Al}_2\text{O}_3 + \text{ZrO}_2$ ceramic partly stabilized with CaO , had pores 2-3 mm in diameter and were preheated to 450°C prior to casting. After casting they were examined under an optical microscope, which revealed clusters of non-metallic inclusions identifiable as titanium nitrides and carbonitride along the boundaries between ceramic phases and steel. A comparison with steel cast without filtering indicated that the filters had, on the average, removed 72.16 % of these inclusions. Also a few exogenous microinclusions of the ceramic material were found in the castings, however, a consequence of filter erosion by steel with a 0.5-0.6 % Ti content. Figures 2; references 6.

Heat-Insulating Zirconium Dioxide-Based Ceramic Coating Advertised

917D0165A Moscow MASHINOSTROITEL in Russian No 3, 1991 p 39

[Unattributed advertisement: "Heat-Insulating Zirconium Dioxide-Based Ceramic Coating"]

[Text] The proposed ceramic coating is applied to the surface of the components of the hot section of gas turbine engines, for example, onto the turbine blade tips of an aviation gas turbine engine.

The coating is characterized by high heat resistance and high adhesion between the ceramic and metal layers at operating temperatures above 1,100°C.

The coating provides increased heat resistance, protects refractory alloys against weakening, makes it possible to obtain a heat-insulating effect of more than 100°C on cooled blades, increases the working temperature of gas in a turbine, and increases engine operating life.

The coating preserves the metallurgical and mechanical properties of the primary blade material during the course of operation at temperatures above 1,100°C, which in turn ensures turbine blading and gas turbine engine reliability.

The coating makes it possible to increase components' durability under conditions of high-temperature gas flows.

The ceramic coating is applied by the method of electron-beam vaporization and condensation of materials in a vacuum onto the surface of new and repaired gas turbine engines.

Main Characteristics of the Zirconium Dioxide-Based Heat-Insulating Ceramic Coating

Surface roughness, μm	$\text{Ra} \leq 1.32$
Heat conduction coefficient, $\lambda^{1,100}$, W/mK	2
Strength of adhesion τ with a metal surface, kgf/mm^2	>5
Coating thickness, μm	up to 200
Operating temperature, °C	900-1,100

Address: 107005, Moscow, NPO VIAM. Telephone: 263-85-72.

COPYRIGHT: Izdatelstvo "Mashinostroyeniye", Mashinostroitel, 1991

Allowing for Defects When Calculating Failure Probability for Ceramic Parts Subjected to Short-Term Loading

917D0157B Kiev PROBLEMY PROCHNOSTI in Russian No 4, 1991 pp 25-30

[Abstract of article by M. I. Gorbatshevich, A. Ye. Ginsburg (Leningrad)]

UDC 539.4.015

[Abstract] The authors adduce equations formulated to estimate the failure probability of ceramic plates. The

equations take into account defect orientation, size, number, and non-linearity. The approach used assumes that ceramic failure is determined by critical unstable growth stresses originating with the most serious defect; in other words, material failure conforms to the "weak link" theory; that ceramic materials are macroscopically isotropic and monolithic and that the presence of cracks does not change the magnitude of macroscopic stresses; i. e., crack dimensions are limited; and that the distributions of the parameters determining critical stresses and of the defect orientation parameters are independent of one another. The equations can be modified to solve for particular states of stress, linear and non-linear loading trajectories, part geometries, and surface treatment of the material. The surface and volume defect values used in these equations can be determined empirically by testing specimens of the representative ceramics. If this information cannot be obtained, then the performance of a ceramic part can be estimated using one of the equations adduced. Examples of how these formulas can be applied are provided. Figures 1; references 11: Russian.

B3

Estimating the Factor of Safety for Ceramic Parts

917D0157A Kiev PROBLEMY PROCHNOSTI in Russian No 4, 1991 pp 20-25

[Abstract of article by Yu. I. Dobrinskiy (Obninsk)]

UDC 666.3.01:539.4

[Abstract] Empirical data describing the strength of ceramic materials and their deterioration as a consequence of slow crack propagation were used to formulate equations to estimate the factor of safety for ceramic parts as a function of bending strength, part size, shape, and volume, and service conditions, particularly subcritical crack propagation. The results of the equations were experimentally verified by subjecting 45 specimens of reaction-bonded silicon nitride ceramic 3 by 3 by 30 cu mm to a three-point bend test. The original strength of the material, taking into account specimen volume, was 274.9 MPa, and the Weibull modulus was 7.06. For these specimens, a 237.5 MPa load yields a theoretical failure probability of 0.3. To avoid ambiguity in the results, acceptable failure probability was set at 0.1. So that the specimens would have a failure probability of 0.1 when subjected to a 237.5 MPa load during the controlled tests, they were pre-tested at 226 MPa. Specimen failure probability at 237.5 MPa during the controlled tests was 0.16 vs the expected 0.1. This discrepancy was attributed to inconsistencies between statistical and actual strength parameters for this batch of specimens and to defects appearing during the course of the tests. The experimental data showed that the theoretical expressions formulated can be used in the design of ceramic structures. Figures 8; references 17: 9 Russian, 8 Western.

Amorphous Materials: Powder-Forming Methods

*917D0173A Minsk DOKLADY AKADEMII NAUK
BSSR in Russian No 1, 1991 pp 51-55*

[Abstract of article by O. V. Roman, corresponding member, Belorussian Academy of Sciences]

UDC 621.762.4

[Abstract] A study was undertaken to determine whether explosive compaction or isentropic compression was more suitable for forming large products from amorphous powder alloys. Explosive compaction was used to form iron- (iron-chromium-phosphorus-carbon) and cobalt-based amorphous powder alloys into specimens that underwent x-ray crystallographic, metallographic, and radiographic analyses. Isentropic compression was used to form specimens from the iron-based powder. Explosive compaction was found to be the only method suitable for forming large products from amorphous alloys, for three major reasons: 1) At forming pressures less than 7 GPa, the equilibrium temperature of the

compacts is lower than the crystallization temperature; 2) The energy released at the interfaces of cylindrical particles 100 μm in diameter and 20 μm thick is sufficient to form a fusion zone 2 to 10 μm in size; 3) The super-fast cooling rate of the fused material in these zones is sufficient to induce secondary amorphization. It was emphasized that this forming method can only be realized under very specific conditions (liquid-phase explosive sintering), a mathematical model of which was provided. A mathematical model for determining the fused surface zones as a proportion of total particle volume was also presented. This model is unique in that it represents a solution to the non-stationary problem of thermal conductivity that takes into account particle finiteness and shape and significant change in the actual thermodynamic characteristics of the amorphous body during temperature changes. While isentropic compression can be used to form large objects from amorphous materials, it results in undesirable structural properties and crystallization behavior. Figures 2; references 13: 11 Russian, 2 Western.

Effect of High-Output Rail Cutting Methods on Resistance Welding Quality

917D0182A Moscow SVAROCHNOYE
PROIZVODSTVO in Russian No 5 (679), May 91
pp 7-9

[Article by N.A. Sinadskiy, V.B. Shlyapin, All-Union Scientific Research Institute of Railway Transport]

UDC 621.791.762.5

[Abstract] The behavior of cross cut end cracks caused by single-point, abrasive, and other types of cutting during the welding of rail joints was examined and the potential danger posed by these cracks was assessed. The study was carried out in bulk quenched R65 rails manufactured by the Nizhniy Tagil Metallurgical Works. Cracks were induced in the rail web by cyclically loading samples in a TsDM-150 pulser. In order to facilitate the

fatigue crack formation, a stress concentrator was developed in the stretched rail web in the form of a structural irregularity produced by an electrode. The cross cut end crack behavior during welding was assessed by the results of visual inspection and metallographically. An analysis of experimental data shows that 2-3 mm long cracks may develop in metal rail ends cut by the abrasive, plasma, anode-mechanical, or friction methods; during flash-butt resistance welding, the metal affected by cracks burns out completely, so these highly efficient cutting methods may be used for the rail welding process. If the crack length exceeds the process allowance for welding, i.e., up to 20 mm per rail end, the cracks propagate further under the effect of residual stresses perpendicular to the crack; consequently, in mixing old and new rails for welding, it is necessary strictly to monitor the presence of longitudinal cracks in the rail web caused by cutting and poor rolling or as a result of operation. References 3; figures 4.

Magnetically Controlled RAP 160/320K-10 X-Ray Unit

*917D0180B Sverdlovsk DEFECTOSKOPIYA in Russian
No 3, Mar 91 pp 60-63*

[Article by Ye.A. Gusev, V.P. Drankov, V.D. Naboyshchikov, Introspection Science Research Institute, Moscow]

UDC 620.179.15

[Abstract] The issue of increasing the reliability of radiography and X-ray metering testing while simultaneously improving the mass and overall dimensions of the X-ray unit is addressed and the use of RUP series X-ray units for this purpose is discussed. The principal circuit of a magnetically controlled RAP-160/320K-10 unit developed by the authors is described. The unit uses a three-phase high-voltage transformer with a magnetic regulator in the main circuit, making it possible to eliminate the X-ray tube lagging which leads to a low anode voltage stability and poor reliability and the need to employ a high-voltage filter. The X-ray unit's external characteristic and performance curve as well as its block diagram are cited. The new unit is compared to the best foreign makes, particularly MC 163/323 by Philips, Isovolt 160/320 by Seifert, and HF 160/320 by Pantak. It is shown that the use of the new X-ray unit in the RI-60TK introscope makes it possible to increase the flaw detectability by 15-20% and raise the inspection efficiency by 25-30%. References 5: 2 Russian, 3 Western; figures 5; tables 1.

Unit for Measuring Dynamic and Quasistatic Magnetic Characteristics

*917D0180A Sverdlovsk DEFECTOSKOPIYA in Russian
No 3, Mar 91 pp 34-39*

[Article by M.A. Melguy, A.A. Osipov, Applied Physics Institute at the Belorussian Academy of Sciences]

UDC 620.179.14

[Abstract] Single- and multiparameter magnetic inspection methods and their advantages and shortcomings are reviewed and the task of improving the methods and facilities of magnetic measurements by means of increasing their accuracy, expanding the magnetization reversal frequency range, and utilizing greater functional capabilities is considered. A new unit developed for measuring such magnetic characteristics as coercive force, remanent induction, peak field and induction, half-cycle of magnetization reversal frequency, differential permittivity, etc., is described. The installation employs a system containing a DVK-1M microcomputer, a CAMAC crate with the necessary set of functional modules, and external input/output and data interchange devices. The central processor (TsP) communicates with RAM (OZU), CAMAC crate, plotter, and external SM-4 computer (EVM) through a standard "Elektronika-60" bus. Measurements may be taken in the manual, interactive, and automatic modes. The measurement procedure and technique are described. The maximum system power demand (without the CAMAC crate, microcomputer, and peripherals) does not exceed 580 mW while the minimum magnetization reversal frequency is 0.035 Hz. An adjusted reproducibility of at least 1.5% was attained. Thus, the possibility of measuring the magnetization reversal rate within 5-1,000 kA/m.s makes it possible to obtain static magnetic characteristics from quasistatic by extrapolating the magnetization field to zero. The software package is written in the DVK-1M microassembler language. References 14; figures 1.

2
NTIS
ATTN PROCESS 103

5285 PORT ROYAL RD
SPRINGFIELD VA

22161

This is a U.S. Government publication. Its contents in no way represent the policies, views, or attitudes of the U.S. Government. Users of this publication may cite FBIS or JPRS provided they do so in a manner clearly identifying them as the secondary source.

Foreign Broadcast Information Service (FBIS) and Joint Publications Research Service (JPRS) publications contain political, military, economic, environmental, and sociological news, commentary, and other information, as well as scientific and technical data and reports. All information has been obtained from foreign radio and television broadcasts, news agency transmissions, newspapers, books, and periodicals. Items generally are processed from the first or best available sources. It should not be inferred that they have been disseminated only in the medium, in the language, or to the area indicated. Items from foreign language sources are translated; those from English-language sources are transcribed. Except for excluding certain diacritics, FBIS renders personal and place-names in accordance with the romanization systems approved for U.S. Government publications by the U.S. Board of Geographic Names.

Headlines, editorial reports, and material enclosed in brackets [] are supplied by FBIS/JPRS. Processing indicators such as [Text] or [Excerpts] in the first line of each item indicate how the information was processed from the original. Unfamiliar names rendered phonetically are enclosed in parentheses. Words or names preceded by a question mark and enclosed in parentheses were not clear from the original source but have been supplied as appropriate to the context. Other unattributed parenthetical notes within the body of an item originate with the source. Times within items are as given by the source. Passages in boldface or italics are as published.

SUBSCRIPTION/PROCUREMENT INFORMATION

The FBIS DAILY REPORT contains current news and information and is published Monday through Friday in eight volumes: China, East Europe, Soviet Union, East Asia, Near East & South Asia, Sub-Saharan Africa, Latin America, and West Europe. Supplements to the DAILY REPORTs may also be available periodically and will be distributed to regular DAILY REPORT subscribers. JPRS publications, which include approximately 50 regional, worldwide, and topical reports, generally contain less time-sensitive information and are published periodically.

Current DAILY REPORTs and JPRS publications are listed in *Government Reports Announcements* issued semimonthly by the National Technical Information Service (NTIS), 5285 Port Royal Road, Springfield, Virginia 22161 and the *Monthly Catalog of U.S. Government Publications* issued by the Superintendent of Documents, U.S. Government Printing Office, Washington, D.C. 20402.

The public may subscribe to either hardcover or microfiche versions of the DAILY REPORTs and JPRS publications through NTIS at the above address or by calling (703) 487-4630. Subscription rates will be

provided by NTIS upon request. Subscriptions are available outside the United States from NTIS or appointed foreign dealers. New subscribers should expect a 30-day delay in receipt of the first issue.

U.S. Government offices may obtain subscriptions to the DAILY REPORTs or JPRS publications (hardcover or microfiche) at no charge through their sponsoring organizations. For additional information or assistance, call FBIS, (202) 338-6735, or write to P.O. Box 2604, Washington, D.C. 20013. Department of Defense consumers are required to submit requests through appropriate command validation channels to DIA, RTS-2C, Washington, D.C. 20301. (Telephone: (202) 373-3771, Autovon: 243-3771.)

Back issues or single copies of the DAILY REPORTs and JPRS publications are not available. Both the DAILY REPORTs and the JPRS publications are on file for public reference at the Library of Congress and at many Federal Depository Libraries. Reference copies may also be seen at many public and university libraries throughout the United States.